PAPER

Check for updates

Electrogenerated chemiluminescence of a Ru(bpy)₃²⁺/arginine system: a specific and sensitive detection of acetaminophen†

Yi Xiao, [ID] [ad] Guofang Wang,[a] Haomin Yi,[a] Suhua Chen,[c] Qinyu Wu,[a] Siyi Zhang,[a] Kexin Deng,[a] Simeng Zhang,[a] Zi-Qi Shi[*b] and Xiaoping Yang [ID] [*a]

Ru(bpy)₃Cl₂/TPrA is a prominent and widely used ECL system in analytical science. However, the co-reactant TPrA restricts the variety of applications because of its toxicity, volatility, and high cost. Here, we use arginine (Arg) as an alternative co-reactant for Ru(bpy)₃²⁺ by taking advantage of its low cost, non-toxicity, and biocompatibility. The mechanism of the Ru(bpy)₃²⁺/Arg system is that the deprotonated Arg can react with Ru(bpy)₃²⁺ to release emission. The similarity between the Ru(bpy)₃²⁺/Arg, Ru(bpy)₃²⁺/TPrA, and Ru(bpy)₃²⁺/DBAE systems demonstrates that Arg can be used as an alternative co-reactant for Ru(bpy)₃²⁺ ECL. As a proof of concept, we achieve an excellent performance for acetaminophen (Ace) detection based on the specificity of Arg and Ace, with excellent linearity, low detection limits, and good recoveries. This work is promising to expand the scope of the Ru(bpy)₃²⁺/Arg system and move forward their applications in bioassays.

1. Introduction

Electrochemiluminescence (ECL) is light emission induced by the electrochemical redox reaction,[1–3] which is an emerging paramount analytical technique with widespread application in the field of analytical applications by virtue of its low background, high sensitivity, simple operation, and excellent spatial/temporal controllability without external light sources.[4–6] A co-reactant is a species that, upon oxidation or reduction, electrochemically generates radicals that can react with ECL luminophores to emit light.[7–9] Due to its wide use in both aqueous and nonaqueous solutions, co-reactant ECL leads to endless potential in analytical applications.[10,11]

As the overwhelming majority of applications concerned co-reactant ECL, the Ru(bpy)₃²⁺/TPrA system forms the basis of commercial systems in biomedical and diagnostic assays[12–14]

due to its outstanding ECL properties, such as high ECL efficiency, high sensitivity and good linearity of response. Tripropylamine (TPrA) is widely used as a co-reactant owing to the merits of high ECL quantum yield, and high electrochemical stability.[15,16] Regardless of its exclusive popularity in ECL, TPrA shows several intrinsic issues such as high toxicity (with low LD₅₀), high volatility (destructive to the human's mucous membrane), and low solubility.[12] Thus, there remains an ultimate need to find an alternative co-reactant for Ru(bpy)₃²⁺ ECL to expand more possibilities in biosensing.

Among the numerous co-reactants,[17] nanomaterial-based co-reactants,[18] 2-(dibutylamino) ethanol (DBAE),[12] amines,[19] and amino acids[20,21] have been widely explored for Ru(bpy)₃²⁺ ECL.[21–23] Arginine (Arg) is a type of amino acid, which possesses a backbone of two primary amines, two secondary amines and one carboxyl. Arg can improve the solubility and biocompatibility for wider biomedical applications, and serve as an effective co-reactant for Ru(bpy)₃²⁺ ECL.[24] However, low ECL efficiency and unclear ECL mechanism have hindered its wider use in biomedical analysis.

Here, we use Arg as an alternate co-reactant for Ru(bpy)₃²⁺ due to its advantages of low cost, non-toxicity, and biocompatibility. We study the mechanism of Ru(bpy)₃²⁺/Arg system, and explore the difference between Ru(bpy)₃²⁺/Arg, Ru(bpy)₃²⁺/TPrA and Ru(bpy)₃²⁺/DBAE systems. As a proof of concept, we apply Ru(bpy)₃²⁺/Arg system for acetaminophen (Ace) analysis, and explore the specific interaction of Arg and Ace. The reliable, economic, and biocompatible Ru(bpy)₃²⁺/Arg system would be a potential powerful tool in analytical applications, and will envision more effective applications.

ᵃKey Laboratory of Study and Discovery of Small Targeted Molecules of Hunan Province, Department of Pharmacy, School of Medicine, Hunan Normal University, Changsha 410013, Hunan, China. E-mail: Xiaoping.Yang@hunnu.edu.cn; shiziqi47@126.com

ᵇAffiliated Hospital of Integrated Traditional Chinese and Western Medicine, Nanjing University of Chinese Medicine, Nanjing 210028, Jiangsu, China

ᶜHunan Provincial Maternal and Child Health Care Hospital, Changsha 410008, Hunan, China

ᵈJohn A. Paulson School of Engineering and Applied Sciences, Harvard University, Cambridge, MA 02138, USA

† Electronic supplementary information (ESI) available: Morphology of MPS, CVs of Ru(bpy)₃²⁺/Arg system, mechanism of Ru(bpy)₃²⁺/TPrA system, CVs of Ru(bpy)₃²⁺/DBAE system, mechanism of Ru(bpy)₃²⁺/DBAE system, repeatability and temperature stability of ECL system. See DOI: 10.1039/d1ra09371a

2. Experimental section

2.1. Chemicals and materials

5,5-Dimethyl-1-pyrroline *N*-oxide (DMPO) is from TCI chemicals. Tris(2,2′-bipyridyl) ruthenium(II) hexahydrate (Ru(bpy)$_3$-Cl$_2$·6H$_2$O, 98%), 2-(dibutylamino) ethanol (DBAE, 99%), tetraethoxysilane (TEOS, ≥99%), bovine serum albumin (BSA, 96%), ammonium hydroxide solution (25 wt%), and tri-*n*-propylamine (TPrA, >99%) are from Sigma-Aldrich Inc. (St Louis, MO, U.S.A). Cetyltrimethylammonium bromide (CTAB, ≥99%) is from Acros Inc. Potassium ferricyanide (K$_3$[Fe(CN)$_6$]), hydroxymethylferrocene (FcMeOH, 97%), arginine (Arg), acetaminophen (Ace), urea (Ur), lactose (Lac), creatinine (Cr), glucose (Glu), sodium chloride (NaCl), potassium chloride (KCl), and magnesium chloride (MgCl$_2$) are from Aladdin Chemical Reagents. L-Tryptophan (Try, 99%), L-tyrosine (Tyr, 99%), L-threonline (Thr, 99%), L-valine (Val, 99%), L-phenylalanine (Phe, 99%), L-histidine (His, 99%), L-alanine (Ala, 99%), L-lysine (Lys, 98%), L-leucine (Leu, 99%), L-glutamine (Glu, 99%), L-proline (Pro, 99%), L-isoleucine (Isol, 99%), L-methionine (Met, 99%), L-aspartic acid (Aspa, 99%), L-asparagine (Asp, 99%), L-serine (Ser, 99%) are from Macklin. Arginine (Arg, >99%), L-(+)-glutamic acid (Glua, 99%), L-cysteien (Cys, 99%), acetaminophen (Ace), hydroquinone (Hyd, 99%), catechol (Cat, 99%) are from Aladdin Chemical Reagents. Glycine (Gla, 99%) are from Shanghai Lanji Technology Development Co., Ltd. Indium tin oxide glass (ITO) is from Kaivo Electronic Components Co., Ltd.

2.2. Preparation of MPS

We pattern the ITO glass by chemical etching.[25,26] We synthesize MPS on the patterned ITO electrode according to the Stöber-solution growth method.[27] The electrochemical and microscopy characterizations of MPS are carried out as described previously.[28] Transmission electron microscopy (TEM) experiments are carried out by a TecnaiG2-F20 transmission electron microscope, and scanning electron microscopy (SEM) experiments by a Hitachi-SU8010 scanning electron microscope. We paste ITO electrode with a paper cover to fabricate the MPS-ECL sensor.

2.3. Experimental procedure

Electrochemistry and ECL imaging experiments are carried out with an electrochemical analyzer (CHI 660E, Shanghai) and an imaging system (Tanon 4600, Shanghai), respectively.

Ultraviolet-visible (UV-vis) absorption spectra are recorded on a UV-2501PC spectrophotometer (Shimadzu). Fluorescence spectra are recorded on a LS 45 luminescence spectrophotometer (PerkinElmer). Emission windows are monitored in the wavelength range of 550–650 nm (λ_{em} = 610 nm) with excitation of 450 nm. Fourier transform infrared spectrometer (FILR) spectra are recorded on a Nicolet 6700 spectrophotometer (Thermo Fisher).

The electrochemical reactions of electron spin resonance (ESR) spectroscopy are performed in 0.1 M PBS (containing 50 μM Ru(bpy)$_3{}^{2+}$, 50 μM Arg, and 10 mM DMPO). A voltage of 1.0 V

is applied to electrolysis for 20 min. ESR spectra are measured using an ESR spectrometer (JES-FA 200). The instrumental parameters are set as follows: a microwave power (0.99800 mW), modulation frequency (9199.688 kHz), sweep width (100 G), modulation amplitude (2 G), center field (3360 G), time constant (6 ms), and scan time (1 min). All experiments are conducted at ~20 °C.

The ECL characterization was performed using PMI-E electrochemiluminescence analysis system (Xi'an Remex Analytical Instrument Co., Ltd). The parameters are set as follows: scan rate (0.05 V s^{-1}), scan range (0.2–1.3 V). PMI-E electrochemical analyzer are used for ECL characterization of Ru(bpy)$_3{}^{2+}$/Arg, Ru(bpy)$_3{}^{2+}$/TPrA and Ru(bpy)$_3{}^{2+}$/DBAE systems. ECL–voltage curves are recorded in a 0.1 M PBS (pH 6.6) containing 9 μM Ru(bpy)$_3{}^{2+}$ and different co-reactants on MPS-ECL sensor.

Recovery experiment was carried out by the standard addition method. 1 mL of sample (containing 10 μM Ru(bpy)$_3{}^{2+}$, 5 μL human serum/saliva and different concentrations of Arg/Ace) was added to the MPS-ECL sensor. We perform the standard addition experiments by adding 500 μM Arg and 150 μM Ace to human serum sample, 300 μM Arg and 50 μM Ace to human saliva sample, respectively. ECL images of 6 sensing spots were acquired simultaneously upon applying a voltage of 2.0 V.

3. Results and discussion

3.1. Electrochemical experiments of Ru(bpy)$_3{}^{2+}$/Arg system

Arg is a type of amino acid, which possesses a backbone of two primary amines, two secondary amines and one carboxyl.[24] Arg can improve the solubility and biocompatibility for wider biomedical applications, and serve as an effective co-reactant for Ru(bpy)$_3{}^{2+}$ ECL. Since electrode material affect the co-reactant ECL, mesoporous silica (MPS) catch our attention owing to the merits of amplification effect of positive ions.[27,29] TEM and SEM images of MPS are displayed in Fig. S1.† MPS are vertically aligned nanochannels (indicated as white pores, 2–3 nm diameter). Compared to that of ITO electrode, MPS electrode can enhance the peak current of Ru(bpy)$_3{}^{2+}$, due to electrostatic attraction.[26]

To reveal the electrochemical behaviors, cyclic voltammograms (CVs) of Arg, Ru(bpy)$_3{}^{2+}$, and Ru(bpy)$_3{}^{2+}$/Arg are investigated. Fig. 1 A shows CVs of blank or Arg solution at MPS electrode with no peaks CV of Ru(bpy)$_3{}^{2+}$ shows a pair of well-defined peaks at MPS electrode, which slightly increased with the addition of Arg. It demonstrates that Ru(bpy)$_3{}^{2+}$ can react more efficiently with Arg, which attributes to the generation of strong ECL emission. Therefore, Arg can enhance the peak current of Ru(bpy)$_3{}^{2+}$ and serve as co-reactant for Ru(bpy)$_3{}^{2+}$ ECL.

Effect of Ru(bpy)$_3{}^{2+}$ concentration on peak current is shown in Fig. 1B. The peak current increases along with the increase of Ru(bpy)$_3{}^{2+}$ concentrations at MPS electrode, while the peak current at ITO electrode displays irregular change along with Ru(bpy)$_3{}^{2+}$ concentration (Fig. S2B†). It indicates that the enhanced peak current at MPS electrode could be used. for sensitive detection of Ru(bpy)$_3{}^{2+}$. Effect of solution pH is shown in Fig. 1C. Due to the isoelectric point of Arg (10.76), oxidation
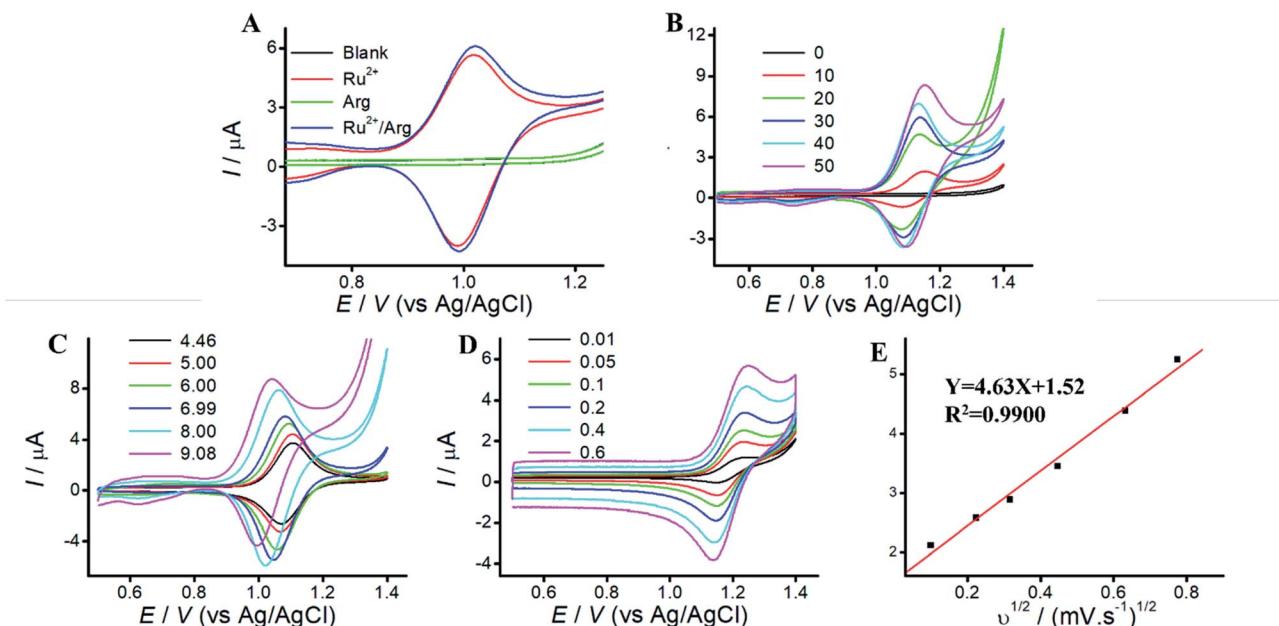
**Fig. 1** Electrochemical experiments of $Ru(bpy)_3^{2+}$/Arg system. (A) CVs of different solutions (in 0.1 M PBS, pH 9.08) at MPS electrode. Scan rate: 0.05 V s^{-1}. (B) CVs of different concentrations of $Ru(bpy)_3^{2+}$ from 0 μM to 50 μM with 50 μM Arg at MPS electrode. (C) CVs of different pH (4.46, 5.00, 6.00, 6.99, 8.00, 9.06) with 50 μM $Ru(bpy)_3^{2+}$ and 50 μM Arg. (D) CVs of different scan rates from 0.01 V s^{-1} to 0.6 V s^{-1} with 50 μM $Ru(bpy)_3^{2+}$ and 50 μM Arg. (E) Linear plot of oxidation peak current vs. $v^{1/2}$.

of Arg occurs easier in alkaline solution. The peak current increases along with the increase of solution pH at MPS electrode. Thus, we choose solution pH 9.05 for the following experiments. Effect of different scan rates are shown in Fig. 1D. The peak current of anodic oxidation increases with the increasing scan rates, and the excellent linear relationship between peak current and $v^{1/2}$ suggests that the ECL process is a diffusion-controlled reaction.

3.2. Characterization of $Ru(bpy)_3^{2+}$/Arg/Ace system

To reveal the mechanism of $Ru(bpy)_3^{2+}$/Arg system, UV-vis experiment is performed. As shown in Fig. 2A, Arg exhibits no UV absorption. Three UV absorption peaks at 242 nm, 290 nm and 470 nm are assigned to $Ru(bpy)_3^{2+}$. Among them, the peaks at 242 nm, 290 nm and 470 nm belong to metal-centered transition, ligand-centered transition, and metal-to-ligand charge transfer of $Ru(bpy)_3^{2+}$, respectively. The absorption peaks of the mixture of $Ru(bpy)_3^{2+}$ and Arg are the sum of individuals. As a proof of concept, we apply $Ru(bpy)_3^{2+}$/Arg system for Ace detection. Fig. 2A clearly illustrates the characteristic UV absorption peak at 244 nm of Ace. With the addition of Ace, an absorption peak at 244 nm appears in the mixture of $Ru(bpy)_3^{2+}$/Arg/Ace.

Fluorescence experiments give the information on characteristic peaks of $Ru(bpy)_3^{2+}$/Arg. As shown in Fig. 2B, Arg and Ace exhibit no fluorescence peak, and the peak of $Ru(bpy)_3^{2+}$ is located at 610 nm. When Arg or Ace is added to $Ru(bpy)_3^{2+}$ solution, the change in fluorescence intensity at 610 nm is almost unobservable.

ESR experiments are performed to identify the electro-generated radical species $H_2N^{\bullet+}CH(C_4N_3H_{11})COO^-$ in $Ru(bpy)_3^{2+}$/Arg system. As shown in Fig. 2C, the electrochemical solution without electrolysis exhibits slight fluctuation with the addition of a spin-trapping agent (DMPO). The solution with electrolysis exhibits three lines, which corresponds to the free electron generated on the nitrogen nuclei N (1 N, $I = 1$). The results suggest that the reaction between Arg and $Ru(bpy)_3^{2+}$ leads to generate $H_2N^{\bullet+}CH(C_4N_3H_{11})COO^-$.

3.3. Possible mechanism of $Ru(bpy)_3^{2+}$/Arg system

The ECL characterizations of $Ru(bpy)_3^{2+}$/Arg, $Ru(bpy)_3^{2+}$/TPrA, and $Ru(bpy)_3^{2+}$/DBAE systems are shown in Fig. 2. Generally, the ECL emission of this system as a function of applied potential. The wave occurs with the direct oxidation of $Ru(bpy)_3^{2+}$ at the electrode. Then $Ru(bpy)_3^{3+}$ react with Arg to generate the positively charged radical. The radical undergoes a deprotonation process to generate the corresponding radical ion, which could react with $Ru(bpy)_3^{3+}$ to emit light. We can observe a significantly big wave in $Ru(bpy)_3^{2+}$/Arg systems, which is associated with the emission from $Ru(bpy)_3^{2+*}$. As shown in Fig. 2, the mechanism of $Ru(bpy)_3^{2+}$/Arg is presumably analogous to that of the $Ru(bpy)_3^{2+}$/TPrA system and $Ru(bpy)_3^{2+}$/DBAE. With the addition of Ace, the ECL intensity significantly decreased in $Ru(bpy)_3^{2+}$/Arg/Ace system, while that of $Ru(bpy)_3^{2+}$/TPrA/Ace system and $Ru(bpy)_3^{2+}$/DBAE/Ace change a little. It demonstrates that $Ru(bpy)_3^{2+}$/Arg is suitable for specific Ace detection.

By taking full accounts of aforementioned results,[7] the ECL mechanism is summarized as follows: $Ru(bpy)_3^{2+}$ is oxidized to generate $Ru(bpy)_3^{3+}$ at MPS electrode, while $Ru(bpy)_3^{3+}$ react
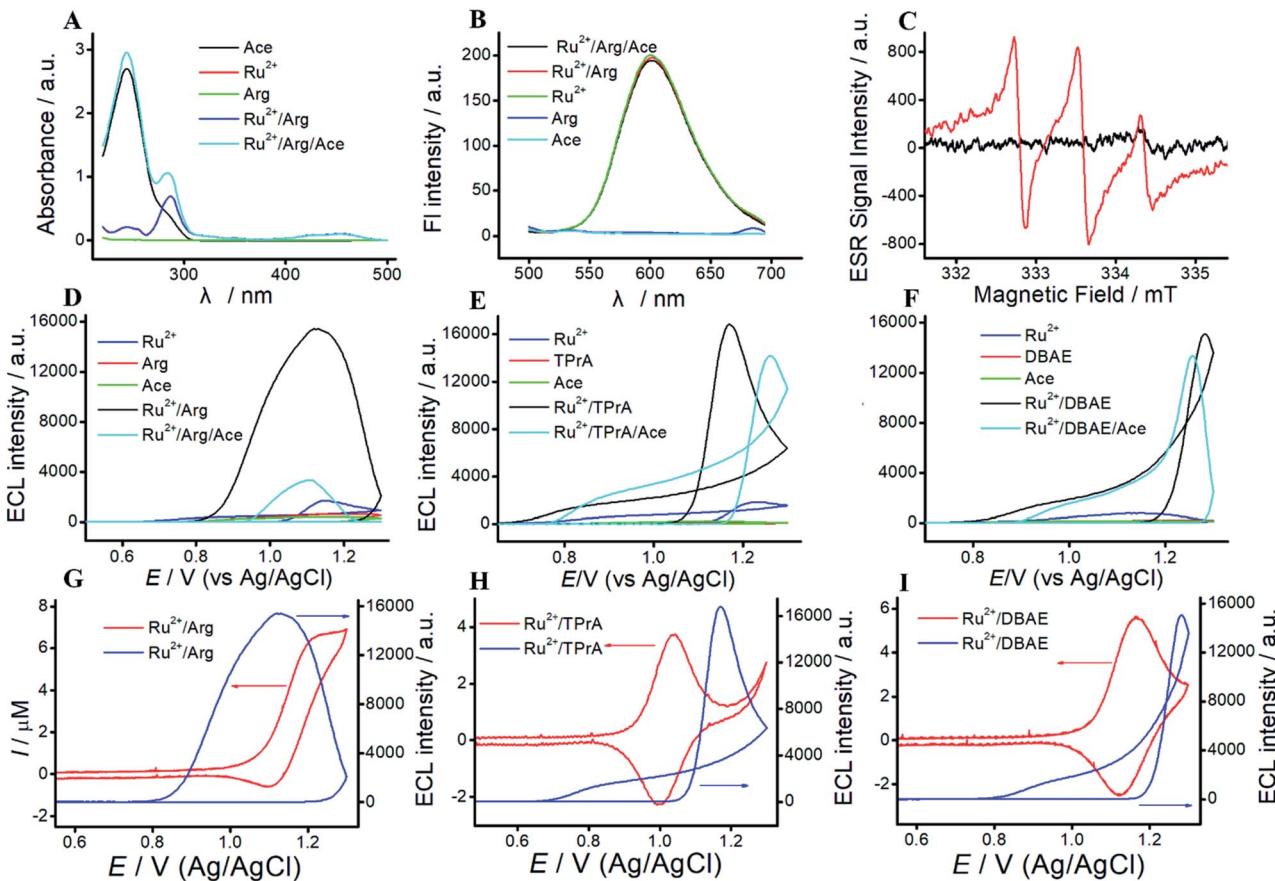
**Fig. 2** Characterization of $Ru(bpy)_3^{2+}$/Arg/Ace system. (A) UV-vis absorption of different solutions (10 μM $Ru(bpy)_3^{2+}$, 50 μM Ace and 50 μM Arg). (B) Fluorescence spectra of different solutions (10 μM $Ru(bpy)_3^{2+}$, 50 μM Ace and 50 μM Arg, λ_{exc} = 452 nm). (C) ESR experimental spectra recorded before electrolysis (black line) and after electrolysis (red line) at 1.0 V with 50 μM $Ru(bpy)_3^{2+}$, 50 μM Arg and 10 μM DMPO (0.1 M PBS, pH = 9.10). (D) ECL coupled with CV in 10 μM $Ru(bpy)_3^{2+}$, 70 μM Arg, 50 μM Ace (0.1 M PBS, pH 9.21) at MPS electrode with scan rate of 0.05 V s^{-1}. (E) 10 μM $Ru(bpy)_3^{2+}$, 10 μM TPrA, and 50 μM Ace. (F) 10 μM $Ru(bpy)_3^{2+}$, 4 μM DBAE, 50 μM Ace. (G) Synchronous response curve of cyclic voltammetry and voltage of 10 μM $Ru(bpy)_3^{2+}$–70 μM Arg system. H. Synchronous response curve of cyclic voltammetry and voltage of 10 μM $Ru(bpy)_3^{2+}$–10 μM TPrA system. (I) Synchronous response curve of cyclic voltammetry and voltage of 10 μM $Ru(bpy)_3^{2+}$–4 μM DBAE system.

with Arg to generate the positively charged radical. The radical undergoes a deprotonation process to generate the corresponding radical ion, which could react with $Ru(bpy)_3^{3+}$ to emit light. The mechanism of $Ru(bpy)_3^{2+}$/Arg is presumably analogous to that of the $Ru(bpy)_3^{2+}$/TPrA system, and can be written as follows:

$$Ru(bpy)_3^{2+} - e^- \rightarrow Ru(bpy)_3^{3+}$$

$$Ru(bpy)_3^{3+} + H_2NCH(C_4N_3H_{11})COOH \rightarrow Ru(bpy)_3^{2+} + H_2NCH(C_4N_3H_{11})COOH^{\bullet+}$$

$$H_2NCH(C_4N_3H_{11})COOH^{\bullet+} \rightarrow H_2NCH(C_4N_3H_{11})COOH^{\bullet} + H^+$$

$$Ru(bpy)_3^{3+} + H_2NCH(C_4N_3H_{11})COOH^{\bullet} \rightarrow [Ru(bpy)_3^{2+}]^* + HN{=}C(C_4N_3H_{11})COO^- + H^+$$
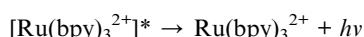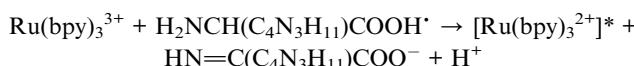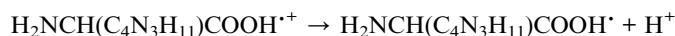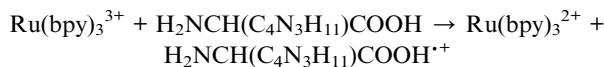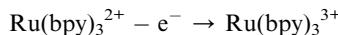
$$[Ru(bpy)_3^{2+}]^* \rightarrow Ru(bpy)_3^{2+} + h\nu$$

3.4. Comparison among $Ru(bpy)_3^{2+}$/TPrA, $Ru(bpy)_3^{2+}$/DBAE and $Ru(bpy)_3^{2+}$/Arg system

To investigate the differences among $Ru(bpy)_3^{2+}$/TPrA, $Ru(bpy)_3^{2+}$/DBAE and $Ru(bpy)_3^{2+}$/Arg system, we study the mechanism of three different systems. For $Ru(bpy)_3^{2+}$/TPrA system (Fig. S3†), CVs of blank or TPrA solution at ITO electrode exhibit no peaks. CV of $Ru(bpy)_3^{2+}$ shows a pair of well-defined peaks at ITO electrode, which increases with the addition of TPrA. Due to the electrostatic attraction, MPS electrode can significantly enhance the peak currents of $Ru(bpy)_3^{2+}$ and $Ru(bpy)_3^{2+}$/Arg solution. Effect of rate scan is shown in Fig. S3C.† The peak current increases along with the increase of scan rate, and there is an excellent linear relationship between the peak current and $\nu^{1/2}$, indicating that ECL process is a diffusion-controlled reaction. UV-vis spectra of TPrA and Ace exhibit absorption peaks at 230 nm and 244 nm, respectively. UV-vis spectra of $Ru(bpy)_3^{2+}$ show three characteristic absorption peaks at 242 nm, 290 nm and 470 nm. With the addition of Ace, a strong absorption peak at 244 nm appears in the mixture

of $Ru(bpy)_3^{2+}$/Arg/Ace. As shown in Fig. S3F,† the fluorescence spectra of TPrA and Ace exhibit no fluorescence peak. And $Ru(bpy)_3^{2+}$, $Ru(bpy)_3^{2+}$/TPrA and $Ru(bpy)_3^{2+}$/TPrA/Ace solution exhibit a fluorescence peak at 610 nm.

For $Ru(bpy)_3^{2+}$/DBAE system (Fig. S4 and S5†), CVs of Ace or DBAE show no current peaks. $Ru(bpy)_3^{2+}$/DBAE and $Ru(bpy)_3^{2+}$/DBAE/Ace system exhibit a redox peak at 1.1 V, which assign to the oxidation of $Ru(bpy)_3^{2+}$, and increase with the increasing Ace concentration (Fig. S4†). The peak current of $Ru(bpy)_3^{2+}$/DBAE/Ace system is higher than that of $Ru(bpy)_3^{2+}$/DBAE system, indicating that $Ru(bpy)_3^{2+}$/DBAE can react with Ace. Due to the electrostatic interaction, MPS electrode can significantly enhance the peak currents of different solutions. As shown in Fig. S5C,† UV absorption of $Ru(bpy)_3^{2+}$/DBAE and $Ru(bpy)_3^{2+}$/DBAE/Ace system are sum of individuals. As shown in Fig. S5D,† the fluorescence spectra of Ace and DBAE exhibit no fluorescent peaks, while that of $Ru(bpy)_3^{2+}$, $Ru(bpy)_3^{2+}$/DBAE, and $Ru(bpy)_3^{2+}$/DBAE/Ace. solutions exhibit a significant fluorescent emission at 610 nm under an excitation wavelength of 450 nm. The results illustrate that the mechanism of $Ru(bpy)_3^{2+}$/Arg is similar with classic co-reactant ECL systems ($Ru(bpy)_3^{2+}$/TPrA and $Ru(bpy)_3^{2+}$/DBAE). Besides, Arg exhibits advantages of low cost, non-toxicity, and biocompatibility. Thus, Arg can serve as an alternative co-reactant for $Ru(bpy)_3^{2+}$ ECL.

3.5. Specific interaction between Arg and Ace

As a proof of concept, we apply the $Ru(bpy)_3^{2+}$/Arg system for Ace detection. As reported previously,[16,30] there is a specific interaction between Arg and Ace based on the formation of as many as four hydrogen bonds. As shown in Fig. 3, the characteristic UV absorption peak of Ace is located at 244 nm, which increases along with the increase of Ace concentration. The peak absorption exhibits an excellent linear relationship with

Ace concentration varying from 1 μM to 180 μM. The linear relationship is $Y = 0.009X + 0.0068$ ($R^2 = 0.9988$). As shown in Fig. 3E, the UV absorption peak of Arg is located at 190 nm, which displays irregular change with Arg concentration. As show in Fig. 3C, UV absorption peaks at 190 nm and 244 nm are assigned to the hydroxyl group and the benzene amides group of the mixture of Arg and Ace, respectively. The absorption peak at 190 nm of the mixture is basically unchanged compared with that of Arg or Ace. With the addition of Arg, the absorption peak at 244 nm of the mixture displays a slight increase (Fig. 3D).

The hydroxyl group of Ace could interact with the amino group of Arg to form hydrogen bonds.[30] The greater number of hydrogen bonds formed attributes to the lower absorbance of hydroxyl group at 199 nm. The maximum number of hydrogen bonds are formed when the ratio of Arg : AP is 50 : 50 (Fig. 3F), which leads to the lowest absorbance.

As shown in Fig. 3G, once excited at 450 nm, Arg and Ace both exhibit a strong fluorescence emission peak at 310 nm. Two peaks located at 305 nm and 330 nm are observed in the mixture of Arg and Ace, indicating the formation of a strong complex between Ace and Arg. Therefore, we can achieve a specific detection of Ace based on the hydrogen bonds formed between Arg and Ace. Various compounds such as Ur, Lac, Cr, Glu, NaCl, KCl, BSA, and $MgCl_2$ are used as the interfering species to evaluate the selectivity of Ace assay. As shown in Fig. 3H, most interfering species exhibit no quenching behavior, while I/I_0 is significantly enhanced with the addition of Ace, illustrating the selectivity of Ace assay.

To evaluate the selectivity of our MPS-ECL sensor, we investigated the ECL intensity and quenching effect of 20 types of amino acids. As shown in Fig. S6,† 11 amino acids exhibit no ECL intensity (gray value < 3000) at concentration of 300 μM, including Try, Tyr, Cys, Ser, Gly, Gluc, Thr, Aspc, Glu, Asp, and Ala. His, Leu, and Phe showed weak ECL intensity at 300 μM
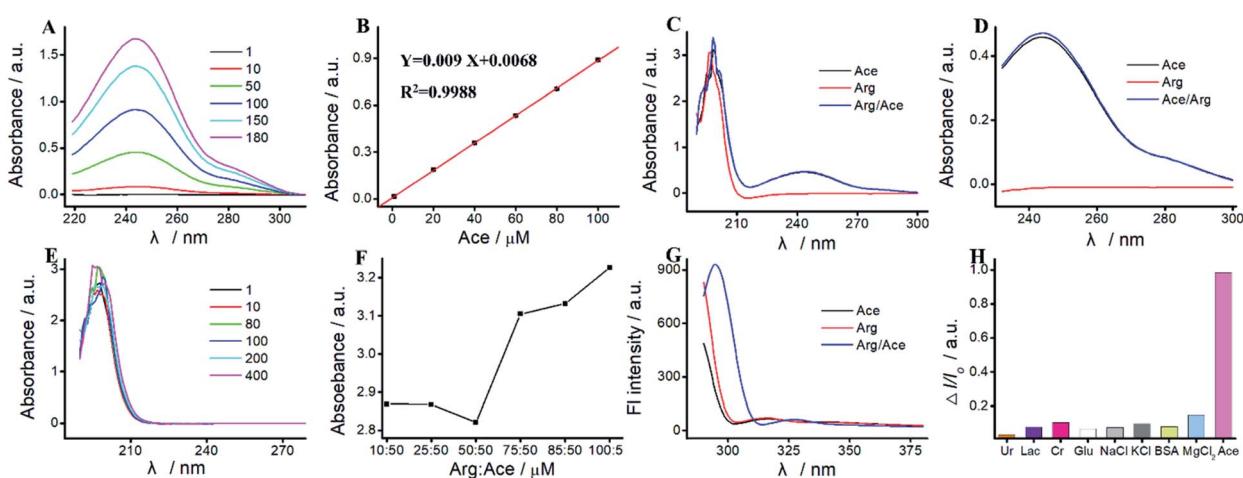

Fig. 3 Specific interaction between Arg and Ace. (A) UV-vis absorption of different Ace concentrations. The concentrations of Ace are from 1 μM to 180 μM. (B) Peak absorbance at 244 nm for different Ace concentrations. The concentrations of Ace are from 1 μM to 180 μM. (C) UV-vis absorption of 50 μM Ace, 50 μM Arg and 50 μM Ace/50 μM Arg solutions. (D) The amplification of UV spectra at 244 nm. (E) UV-vis absorption of different Arg concentrations. (F) Peak absorbance at 199 nm at different ratio of Ace and Arg. The concentrations of Arg are from 1 μM to 400 μM. (G) Fluorescence spectra of 50 μM Ace, 50 μM Arg and 50 μM Ace/50 μM Arg solutions excited at 290 nm. (H) Effect of different interfering species (containing 10 μM $Ru(bpy)_3^{2+}$, 70 μM Arg and 50 μM of different interfering species) on ECL intensity.

(3000 < gray value < 8000). Iso, Arg, Met, Lys, Val, and Pro yielded high ECL intensity at 300 μM (10 000 < gray value).

Besides, we apply $Ru(bpy)_3^{2+}$/amino acid systems for Ace detection. As shown in Fig. S6,† 11 amino acids generated weak quenching efficiency ($0 < \Delta I/I_0 < 0.5$), including Pro, Try, Tyr, Asp, Ser, Glu, Gluc, Thr, Ala, Gly, and Aspc. Cys, Phe, His, Met, Val, Leu, Lys, Arg, and Iso yielded high quenching efficiency ($0.5 < \Delta I/I_0$). The selectivity of our MPS-ECL sensor is shown at Fig. S6.† $Ru(bpy)_3^{2+}$/Arg system exhibits high ECL intensity, and high quenching efficiency for Ace detection.

3.6. Determination of Arg

We apply $Ru(bpy)_3^{2+}$/Arg system for Arg detection. As shown in Fig. 4 and Table S1,† ECL intensity increases along with the increase of Arg concentration in the range of 1 μM–700 μM. The linear relationship can be expressed as $Y = 88.55X + 4653.91$ ($R^2 = 0.9974$). The detection limit (LOD) of Arg is calculated as 0.59 μM (S/N = 3). The quantitation limit (LQD) is calculated as 1.97 μM (S/N = 10). We apply $Ru(bpy)_3^{2+}$/TPrA system for TPrA detection. Fig. 4C and D show an excellent linear relationship between ECL intensity and TPrA concentration in the range of 0.1 μM–30 μM, where the linear equation is $Y = 1811.79X + 4564.30$ ($R^2 = 0.9839$). LOD and LQD of TPrA are 23.5 nM and 78.33 mM, respectively. We apply $Ru(bpy)_3^{2+}$/DBAE system for DBAE detection. Fig. 4E and F show an excellent linear relationship between ECL intensity and DBAE concentration in the range of 0.5 mM–20 mM, where the linear equation is $Y = 3169.74X + 3652.29$ ($R^2 = 0.9928$). LOD and LOQ of DBAE are 27.3 nM and 91.0 nM, respectively. Although ECL intensity of $Ru(bpy)_3^{2+}$/Arg system isn't as higher as that of $Ru(bpy)_3^{2+}$/TPrA or $Ru(bpy)_3^{2+}$/DBAE systems, Arg is an effective and promising co-reactant for $Ru(bpy)_3^{2+}$ ECL. Arg has better biocompatibility,

good water solubility and lower toxicity, therefore it is promising for potential practical applications.

3.7. Determination of Ace

We apply $Ru(bpy)_3^{2+}$/Arg system for Ace detection. As shown in Fig. 5 and Table S2,† ΔI_{ECL} displays an excellent relationship with Ace concentration within the range of 1 mM–700 mM. The linear relationship is $Y = 0.00202 - 0.00907X$, $R^2 = 0.9828$. For $Ru(bpy)_3^{2+}$/TPrA system, ΔI_{ECL} displays an excellent relationship with Ace concentration within the range of 1 mM–500 mM. The linear relationship is $Y = 0.0018X - 0.5225$, $R^2 = 0.9877$. For $Ru(bpy)_3^{2+}$/DBAE system, ΔI_{ECL} displays an excellent relationship with Ace concentration within the range of 1 mM–500 mM. The linear relationship is $Y = 0.00176X - 0.4190$, $R^2 = 0.9611$. Compared to $Ru(bpy)_3^{2+}$/TPrA and $Ru(bpy)_3^{2+}$/DBAE systems, $Ru(bpy)_3^{2+}$/Arg is effective and specific for Ace detection. The mechanism of $Ru(bpy)_3^{2+}$/Arg is similar with classic coreactant ECL systems ($Ru(bpy)_3^{2+}$/TPrA and $Ru(bpy)_3^{2+}$/DBAE). While $Ru(bpy)_3^{2+}$/TPrA/DBAE generated weak quenching efficiency ($0 < \Delta I/I_0 < 0.6$), $Ru(bpy)_3^{2+}$/Arg system yielded high quenching efficiency ($0 < \Delta I/I_0 < 1$). Compared to $Ru(bpy)_3^{2+}$/TPrA and $Ru(bpy)_3^{2+}$/DBAE systems, $Ru(bpy)_3^{2+}$/Arg is effective and specific for Ace detection. Arg exhibits advantages of low cost, non-toxicity, and biocompatibility in comparison to TPrA's high toxicity, high volatility, and low solubility. It can improve the solubility and biocompatibility for wider biomedical applications, and serve as an effective co-reactant for $Ru(bpy)_3^{2+}$ ECL. The limitation of Arg is low ECL quantum yield, and not widely used in ECL in comparison to TPrA's high ECL quantum yield, high electrochemical stability, and exclusive popularity in ECL.

We perform the standard addition experiments by adding 500 mM Arg and 150 mM Ace to human serum sample, 300 mM Arg and 50 mM Ace to human saliva sample respectively. As
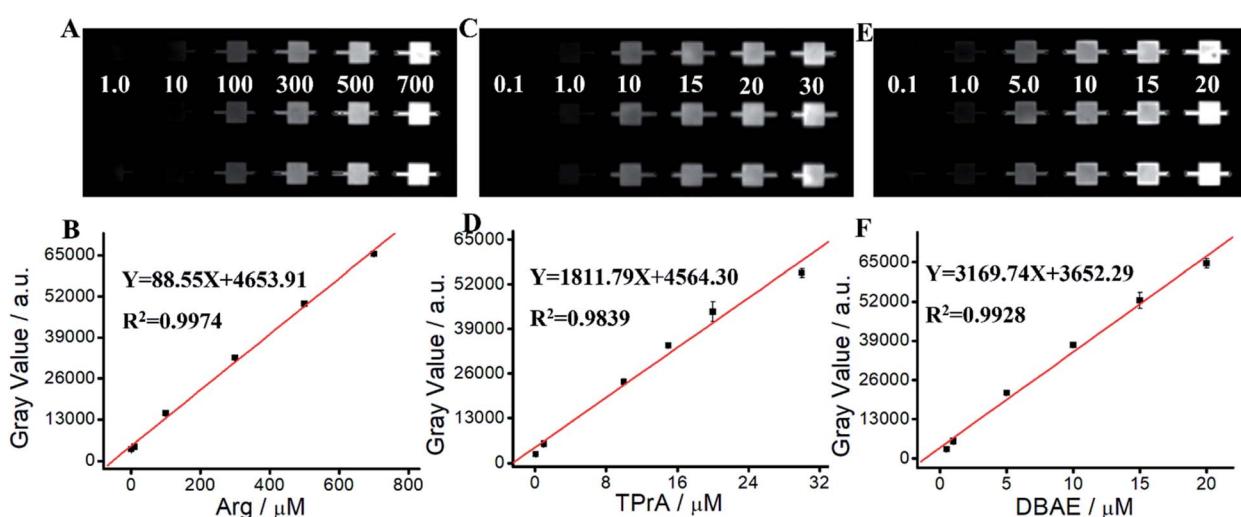

Fig. 4 Determination of different co-reactants. (A) ECL images of different Arg concentrations. The concentrations of Arg are from 1 μM to 700 μM. (B) Calibration curves of different Arg concentrations. The concentrations of Arg are from 1 μM to 700 μM. (C) ECL images of different TPrA concentrations. The concentrations of TPrA are from 0.1 μM to 30 μM. (D) Calibration curves of different TPrA concentrations. The concentrations of TPrA are from 0.1 μM to 30 μM. (E) ECL images of different DBAE concentrations. The concentrations of DBAE are from 0.1 μM to 20 μM. (F) Calibration curves of different DBAE concentrations. The concentrations of DBAE are from 0.1 μM to 20 μM.

© 2022 The Author(s). Published by the Royal Society of Chemistry
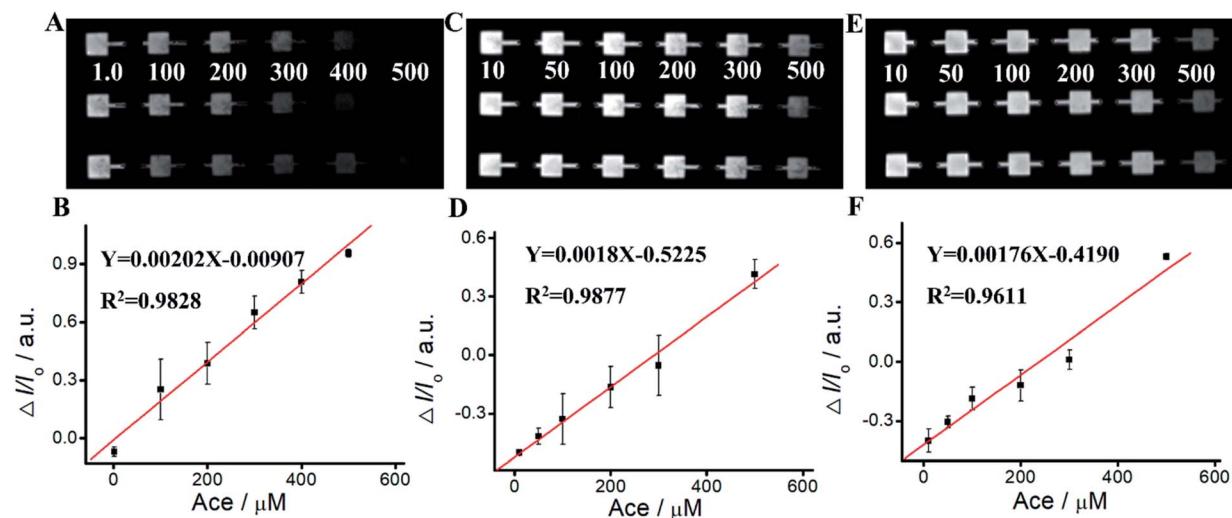
Fig. 5 Determination of Ace. (A) ECL images of different Ace concentrations by 10 μM Ru(bpy)$_3^{2+}$/70 μM Arg system. (B) Calibration curves of different Ace concentrations by 10 μM Ru(bpy)$_3^{2+}$/70 μM Arg system. (C) ECL images of different Ace concentrations by 10 μM Ru(bpy)$_3^{2+}$/20 μM TPrA system. (D) Calibration curves of different Ace concentrations by 10 μM Ru(bpy)$_3^{2+}$/20 μM TPrA system. (E) ECL images of different Ace concentrations by 10 μM Ru(bpy)$_3^{2+}$/10 μM DBAE system. (F) Calibration curves of different Ace concentrations by 10 μM Ru(bpy)$_3^{2+}$/10 μM DBAE system.

shown in Fig. 6, Tables S3 and S4,† satisfied recovery of 93.50% with RSD 0.58% for Arg detection in human serum, and 109.22% with RSD 1.89% for Ace detection are obtained, exhibiting excellent high reliability of the ECL system. We also get good recoveries for Arg and Ace detection in human saliva.

We compared our method with conventional HPLC-UV for human serum and saliva analysis. As shown in Tables S5 and S6,† both of the methods showed good dynamic ranges and coefficient with $R > 0.99$. And MPS-ECL sensor showed a comparative performance to conventional HPLC-UV in determination accuracy. Our MPS-ECL sensor offers an alternative method for Ace detection with relatively high sensitivity.

3.8. Reproducibility and repeatability

To evaluate the practicability and reliability of the ECL system, we measure the ECL intensity of 50 mM Arg at five different sensors. As shown in Fig. S7,† RSD value is 4.61%, suggesting a satisfactory reproducibility of the ECL system between different batches. The thermal stability is evaluated by measuring the ECL intensity at different temperature, varying from −25 °C to 100 °C. Fig. S7† depicts the corresponding results, and ECL intensities almost keep a stable situation. RSD is 4.30%, indicating the ECL system has an excellent thermal stable.
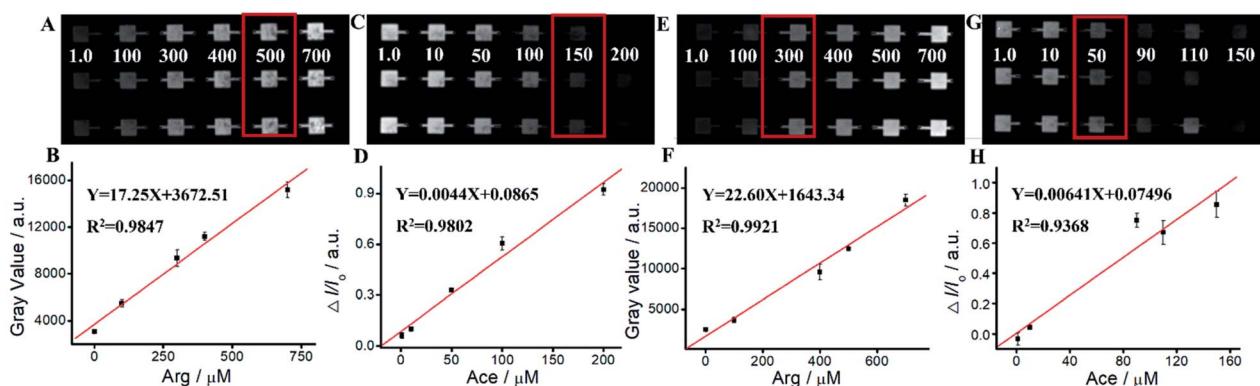

Fig. 6 Recovery of standard addition method. (A and B) ECL images and calibration curves of Arg detection in human serum (containing 10 μM Ru(bpy)$_3^{2+}$, 5 μL human serum and different concentrations of Arg). (C and D) ECL images and calibration curves of Ace detection in human serum (containing 10 μM Ru(bpy)$_3^{2+}$, 5 μL human serum, 70 μM Arg and different concentrations of Ace). (E and F) ECL images and calibration curves of Arg detection in human saliva (containing 10 μM Ru(bpy)$_3^{2+}$, 5 μL human saliva and different concentrations of Arg). (G and H) ECL images and calibration curves of Ace detection in human saliva (containing 10 μM Ru(bpy)$_3^{2+}$, 5 μL human saliva, 70 μM Arg and different concentrations of Ace.

4. Conclusions

We use Arg as an alternate co-reactant for $Ru(bpy)_3^{2+}$ because of its low cost, biocompatibility, and non-toxicity. The mechanism of $Ru(bpy)_3^{2+}$/Arg system is that the deprotonated Arg can react with $Ru(bpy)_3^{2+}$ to release emission. The similarity between $Ru(bpy)_3^{2+}$/Arg, $Ru(bpy)_3^{2+}$/TPrA, and $Ru(bpy)_3^{2+}$/DBAE systems demonstrates that Arg can be used as an alternative co-reactant for $Ru(bpy)_3^{2+}$ ECL. Selective detection of Ace is achieved based on the specific interaction of Arg and Ace, which forms four hydrogen bonds between Arg and Ace. Sensitive Ace assay verifies the accuracy and practicability of $Ru(bpy)_3^{2+}$/Arg system, with excellent linearity, low LODs and good recoveries. Arg exhibits advantages of low cost, non-toxicity, and biocompatibility in comparison to TPrA's high toxicity, high volatility, and low solubility. It can improve the solubility and biocompatibility for wider biomedical applications, and serve as an effective co-reactant for $Ru(bpy)_3^{2+}$ ECL. The limitation of Arg is low ECL quantum yield, and not widely used in ECL in comparison to TPrA's high ECL quantum yield, high electrochemical stability, and exclusive popularity in ECL. This reliable, economic, and biocompatible ECL system would be a potential powerful tool in analytical applications.

Author contributions

Yi Xiao: conceptualization, methodology, investigation, writing – original draft, review & editing, funding acquisition. Guofang Wang: methodology, data curation. Haomin Yi: methodology. Suhua Chen: conceptualization, resources, review & editing. Qinyu Wu: methodology. Siyi Zhang: methodology. Kexin Deng: methodology. Simeng Zhang: visualization, software. Zi-Qi Shi: supervision, funding acquisition. Xiaoping Yang: supervision, funding acquisition.

Conflicts of interest

The authors declare that they have no known competing financial interests or personal relationships that could have appeared to influence the work reported in this paper.

Acknowledgements

Notes and references

1 C. Ma, Y. Cao, X. D. Gou and J. J. Zhu, *Anal. Chem.*, 2020, **92**, 431–454.

2 Z. Y. Liu, W. J. Qi and G. B. Xu, *Chem. Soc. Rev.*, 2015, **44**, 3117–3142.

3 Y. M. Ma, C. Colin, J. Descamps, S. Arbault and N. Sojic, *Angew. Chem., Int. Ed.*, 2021, **60**, 18742–18749.

4 W. L. Guo, H. Ding, P. Zhou, Y. F. Wang and B. Su, *Angew. Chem., Int. Ed.*, 2020, **59**, 6745–6749.

5 X. G. Ma, W. Y. Gao, F. X. Du, F. Yuan, J. Yu, Y. R. Guan, N. O. Sojic and G. B. Xu, *Acc. Chem. Res.*, 2021, **54**, 2936–2945.

6 W. L. Guo, P. Zhou, L. Sun, H. Ding and B. Su, *Angew. Chem., Int. Ed.*, 2021, **60**, 2089–2093.

7 W. Miao, *Chem. Rev.*, 2008, **108**, 2506–2553.

8 L. Z. Hu and G. B. Xu, *Chem. Soc. Rev.*, 2010, **39**, 3275–3304.

9 A. Zanut, A. Fiorani, S. Canola, T. Saito, N. Ziebart, S. Rapino, S. Rebeccani, A. Barbon, T. Irie, H. P. Josel, F. Negri, M. Marcaccio, M. Windfuhr, K. Imai, G. Valenti and F. Paolucci, *Nat. Commun.*, 2020, **11**, 9.

10 Y. He, W. Lian, L. Ding, X. Fan, J. Ma, Q. Y. Zhang, X. Ding and G. Lin, *Arch. Toxicol.*, 2021, **95**, 103–116.

11 W. X. Lv, H. C. Ye, Z. Q. Yuan, X. J. Liu, X. Chen and W. S. Yang, *TrAC, Trends Anal. Chem.*, 2020, **123**, 10.

12 X. Q. Liu, L. H. Shi, W. X. Niu, H. J. Li and G. B. Xu, *Angew. Chem., Int. Ed.*, 2007, **46**, 421–424.

13 M. Sentic, M. Milutinovic, F. Kanoufi, D. Manojlovic, S. Arbault and N. Sojic, *Chem. Sci.*, 2014, **5**, 2568–2572.

14 Z. Q. Ning, E. L. Yang, Y. J. Zheng, M. Y. Chen, G. Q. Wu, Y. J. Zhang and Y. F. Shen, *Anal. Chem.*, 2021, **93**, 8971–8977.

15 N. S. Adamson, A. G. Theakstone, L. C. Soulsby, E. H. Doeven, E. Kerr, C. F. Hogan, P. S. Francis and L. Dennany, *Chem. Sci.*, 2021, **12**, 9770–9777.

16 W. Miao, J.-P. Choi and A. J. Bard, *J. Am. Chem. Soc.*, 2002, **124**, 14478–14485.

17 M. Saqib, S. Bashir, H. J. Li, C. P. Li, S. S. Wang and Y. D. Jin, *Anal. Chem.*, 2019, **91**, 12517–12524.

18 Y. Chen, X. D. Gou, C. Ma, D. C. Jiang and J. J. Zhu, *Anal. Chem.*, 2021, **93**, 7682–7689.

19 S. Carrara, F. Arcudi, M. Prato and L. De Cola, *Angew. Chem., Int. Ed.*, 2017, **56**, 4757–4761.

20 Y. He, Y. Q. Chai, R. Yuan, H. J. Wang, L. J. Bai, Y. L. Cao and Y. L. Yuan, *Biosens. Bioelectron.*, 2013, **50**, 294–299.

21 L. L. Liu, J. C. Bao, M. Fang, L. F. Li and Z. H. Dai, *Sens. Actuators, B*, 2009, **139**, 527–531.

22 M. Saqib, S. Bashir, S. A. Kitte, H. J. Li and Y. D. Jin, *Chem. Commun.*, 2020, **56**, 5154–5157.

23 J. G. Li, Q. Y. Yan, Y. L. Gao and H. X. Ju, *Anal. Chem.*, 2006, **78**, 2694–2699.

24 M. Zhao, X. Chai, J. Han, G. F. Gui, R. Yuan and Y. Zhuo, *Anal. Chim. Acta*, 2014, **846**, 36–43.

25 S. Wu, Z. Zhou, L. Xu, B. Su and Q. Fang, *Biosens. Bioelectron.*, 2014, **53**, 148–153.

26 Y. Xiao, L. R. Xu, P. Li, X. C. Tang and L. W. Qi, *Anal. Chim. Acta*, 2017, **983**, 96–102.

27 Z. G. Teng, G. F. Zheng, Y. Q. Dou, W. Li, C. Y. Mou, X. H. Zhang, A. M. Asiri and D. Y. Zhao, *Angew. Chem., Int. Ed.*, 2012, **51**, 2173–2177.

28 A. Walcarius, E. Sibottier, M. Etienne and J. Ghanbaja, *Nat. Mater.*, 2007, **6**, 602–608.

29 F. Yan, Y. Y. He, L. H. Ding and B. Su, *Anal. Chem.*, 2015, **87**, 4436–4441.

30 Y. Zhang, Z. Y. Huang, L. T. Wang, C. M. Wang, C. D. Zhang, T. Wiese, G. D. Wang, K. Riley and Z. Wang, *Anal. Chem.*, 2018, **90**, 4733–4740.